Supporting Information for "Identifying structural signatures of shear banding in model polymer nanopillars"

Robert J. S. Ivancic[1] and Robert A. Riggleman[2]

[1]Department of Physics and Astronomy, University of Pennsylvania, Philadelphia, PA 19104
[2]Department of Chemical and Biomolecular Engineering, University of Pennsylvania, Philadelphia, PA 19104

1 Additional details about plane weakness models

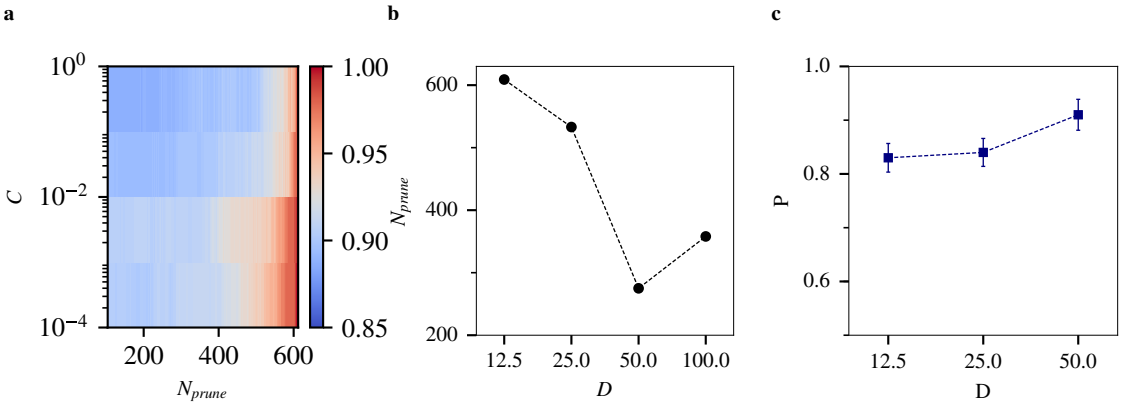

Figure 1: **Details of plane weakness models. (a)** 3-fold cross-validation accuracy is plotted against C and N_{prune} for the $D = 12.5$ pillar diameter. **(b)** Plot of N_{prune} as a function of pillar diameter. **(c)** Test set accuracy for smallest three pillar diameters when tested on the model that was trained at the largest pillar diameter ($D = 100$).

Here, we provide additional details about the plane weakness models. Figure S1a shows a typical plot of plane weakness 3-fold cross-validation accuracies (the percentage of correctly classified planes with the highest and lowest $\langle J_2 \rangle_i$ in each pillar) as a function of both our hyperparameters, C and N_{prune}. Note that test set accuracies are typically $1-2$ percent less than these values due to a slight amount of overfitting. We find that increasing the number of pruned structure functions moderately increases cross-validation scores indicating that our model improves as we prune more structure functions but does not change much so long as $C < 10^{-2}$. We now turn to a plot of the number of pruned structure functions against pillar diameter, Figure S1b. We find that this number generally decreases with increasing pillar diameter. This suggests that a greater number of structure functions are predictive of shear band formation as pillar diameter increases.

While our models are are clearly independent in the sense that they are trained on independent sets of data, we have not shown that they are statistically independent. To determine this, we plot the test set accuracy of the three smallest pillars for a model trained exclusively on data from the largest pillar diameter, $D = 100$. If the models are statistically the same, we would expect to see similar test-set accuracies as the largest pillar diameter (99 ± 1 percent). Instead, we see a large decrease in test set accuracy to 91 ± 3 percent for the $D = 50$ pillar. Moreover, as expected test set accuracy decreases as we decrease pillar diameter and

our models diverge even more. At the smallest pillar diameter the test set accuracy is only 83 ± 3 percent. This suggests that, indeed, our models are truly statistically independent.

2 Additional $P(SB|W)$ curves

In Figure S2, we include the $P(SB|W)$ curves for the intermediate pillar diameters $D = 25$ and $D = 50$. We note that they are roughly exponential and similar in nature to the curves at the smallest and largest pillar diameters.

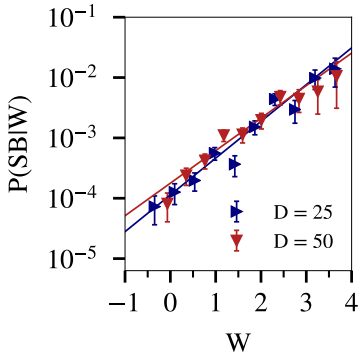

Figure 2: $P(SB|W)$ **for intermediate pillar diameters.** Plots plane weakness, W, against the proability that a plane will shear band given that plane weakness $P(SB|W)$ for the intermediate pillar diameters. These plots are similar in nature to the plots in Figure 2b.

3 Surface fluctuation depth

To measure the depth of the fluctuations causing shear banding on the surface of our pillars, we fit the average radial density structure functions (as shown in Figure 3a for $D = 100$) to the functional form

$$\langle \tilde{G}_{R,i}\left(i; 3.00, 1.00, R\right)\rangle = \frac{A_i}{2}\left(1 + \tanh\left(\alpha_i\left(R - \langle r\rangle_i\right)\right)\right) \tag{1}$$

at each pillar diameter. Here the constants A_i, α_i, and $\langle r\rangle_i$ are fitting parameters. The parameter i denotes whether the fit is for the average over all planes ($i = All$) or shear band planes ($i = SB$). We measure the surface fluctuation depth of the average shear band by considering the quantity $\langle r\rangle_{All} - \langle r\rangle_{SB}$ in Figure S3. These values are impressively small. This quantity obtains its maximum value at $D = 100$ where it is 0.43 and its minimum value at $D = 50$ where it is 0.22. We find no general trend in these data.

4 Density fluctuation width

The width of the density fluctuations may be shown by plotting

$$\Delta G_h\left(h\right) = \langle \tilde{G}_h\left(i; 1.00, h\right)\rangle_{SB} - \langle \tilde{G}_h\left(i; 1.00, h\right)\rangle_{All} \tag{2}$$

for each pillar diameter in Figure S4a. Interestingly, we see for small pillar diameters that these functions are greater than 0 at large h indicating that they have greater than average density. We believe this is a finite size effect due to the the large extent of these surface fluctuations.

To understand the width of these fluctuations, we plot the $h^* = \{h : \Delta G_h\left(h\right) = \Delta G_h\left(1.0\right)/2\}$ against pillar diameter in Figure S4b. We see the width of these fluctuations are increasing sublinearly. The line in Figure S4b corresponds to the power law line of best fit which has an exponent of 0.54.

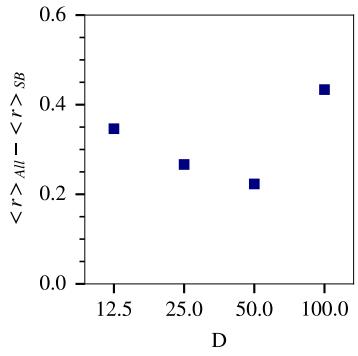

Figure 3: **Surface fluctuation depth as a function of pillar diameter.** Plots of $\langle r \rangle_{All} - \langle r \rangle_{SB}$ as a function of pillar diameter D.

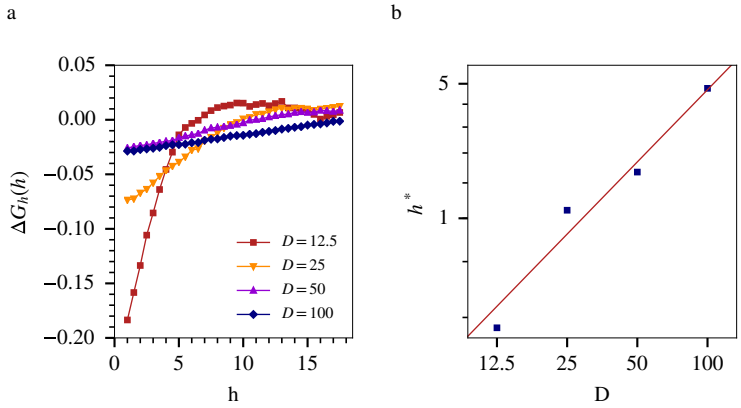

Figure 4: **Surface fluctuation width as a function of pillar diameter. (a)** Plots of $\Delta G_h\,(h)$ at each studied pillar diameter. **(b)** Plots h^*, a length scale which characterizes the width of the density fluctuations, against each studied pillar diameter with power law line of best fit.

5 Assumption of normality of structure functions

When using FIRM and MFIRM metrics in this paper, we have made the assumption that our structure functions follow a multivariate normal distribution. If our structure functions deviate significantly from this assumption, the approximate FIRM scores presented here may deviate significantly from their correct values. To check how well this assumption holds, we will consider the necessary condition that each individual structure funciton is normally distributed. To this end, we first consider the skewness (γ_1) and excess kurtosis (γ_2) of each structure function of a $D = 100$ pillar in Figure S5a. For a perfectly normal distribution, these values would be 0 for all structure functions. Indeed, we find $\gamma_1 \approx 0$ and $\gamma_2 \approx 0$ for the vast majority of structure functions.

We note that 27 structure functions have values skewness or excess kurtosis outside of the range shown in Figure S5a. To examine these more closely, we plot the distributions of the structure functions with the 3 most non-normal skews and excess kurtosis in Figure S5b. For each of these distributions, we have normalized them so they have means of 0 and variances of 1 as indicated by the bar above the structure functions. The worst of these distributions has a unimodal distribution with a large skew (2.6) and excess kurtosis (9.3). These structure functions correspond to R values which are much larger than the nominal radii of the pillar and thus, rarely have values above 0. This indicates that we may expect significant error in our FIRM scores for the largest R values for radial density structure functions. It is important to note, however, that these structure functions are not chosen in our RFE algorithm and thus, we do not expect them to effect the results of FIRM overall. Next, let us look at the distributions of the 4^{th}, 6^{th}, 10^{th}, and

20^{th} most non-normal distributions in Figure S5c. These distributions look reasonably normal and seem to be quickly converging to a normal distribution. Based on these observations and because our models are based on tens or hundreds of structure functions, we believe that our second order approximation to FIRM is quite reasonable for this work. Similar results hold at other pillar diameters.

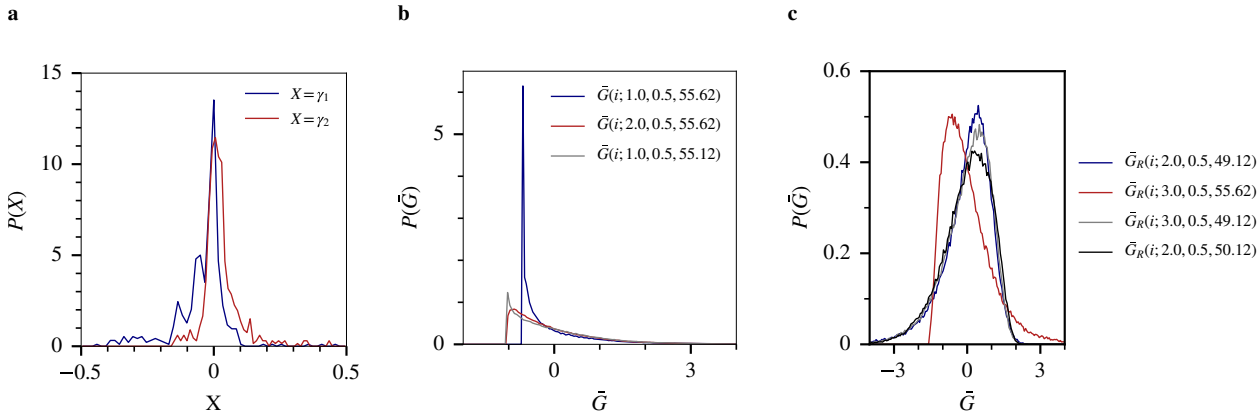

Figure 5: **Testing the normality of our structure functions. (a)** Plots the distribution of skews (γ_1) and excess kurtosis (γ_2). **(b)** Distributions of the most non-normal structure functions. Here, the bar above the structure function indicates that we have normalized them to have 0 mean and unit variance. **(c)** Distributions of the 4^{th}, 6^{th}, 10^{th}, and 20^{th} most non-normal structure function distributions respectively.

6 Effects of additional softness structure functions on fluctuation models

Results from the main text demonstrate that an increase in mean softness local to a given plane increases the probability that the plane will shear band independent of correlations with fluctuations on the plane's surface and internal density fluctuations. One can now postulate that certain configurations of mean softness in the plane may increase the probability that the plane will shear band even further. To test this hypothesis, we fit a multiple linear regression model of all softness structure functions *except* the plane softness structure functions that describe mean softness for $h \leq 1.5$ to the plane density structure functions, radial density structure functions, *and* plane softness structure functions for $h \leq 1.5$. We then proceed to build a fluctuation model based on this multiple linear regression in the manner described in the main text. Thus, this model checks if specific configurations of softness structure functions are predictive of shear banding absent of any correlation with surface fluctuations, internal density or mean softness near the plane. We plot the test set accuracy at each pillar diameter in Figure S6. We find that these models do no better than chance (50 percent). This provides evidence that softness far from the plane and specific configurations of softness within the plane are not predictive of shear banding in pillars of this size.

7 Parameters for local structure functions

To fully define softness, we need to define the parameters used to characterize local structure around particles. We use two parameters to define local structure functions in the Ψ_R family: μ and L. We take $L = 0.05$ for all of these structure functions and have $\mu \in \{0.25, 0.30, 0.35, ..., 2.45\}$. For the Ψ_A family, there are three parameters: ξ, λ, and ζ. We take these parameters to be every unique tuple from the following sets: $\xi \in \{1.0, 1.5, 2.0\}$, $\lambda \in \{-1, 1\}$, and $\zeta \in \{1.000,\ 1.122,\ 1.265,\ 1.434,\ 1.635,\ 1.878,\ 2.174,\ 2.541,\ 3.003,\ 3.597,\ 4.377,\ 5.432,\ 6.906,\ 9.057,\ 12.369,\ 17.863,\ 27.976,\ 49.826,\ 112.253,\ 449.360\}$. Classification accuracy is insensitive to the exact set of parameters used so long as they adequately capture the local structure around particles.

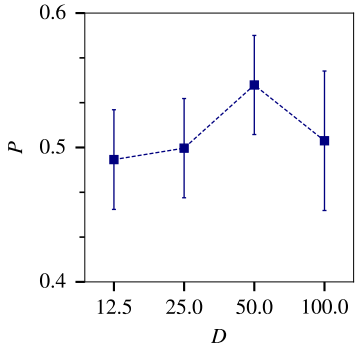

Figure 6: **Fluctuation models of all other softness structure functions.** Plots the test set accuracy of based on fluctuation models of all softness structure functions except the plane softness structure functions that describe mean softness for $h \leq 1.5$ against pillar diameter. The linear regression for these fluctuation models were based on the radial and plane density structure functions as well as the plane softness structure functions $h \leq 1.5$ from the plane.

8 Parameters for structure functions

The structure functions used in this text are parameterized by several variables including: L_R, ξ_h, ξ_R, h, and R. For each family of structure functions, we describe the corresponding density and softness categories of structure functions as with the same parameters. For the plane family of structure functions (G_h and Γ_h), we take $\xi_h = 0.5$ and $h \in \{0, 0.5, 1.0, ..., 18.0\}$. For the radial family of structure functions (G_R and Γ_R), we take $L_R = 0.5$. We then take every unique pair of ξ_h and R such that $\xi_h \in \{1.0, 2.0, 3.0\}$ and $R \in \{D/2 - 5, D/2 - 5 + L_R, ..., D/2 + 4\}$. For the angular structure functions ($G_{A,a}$ and $\Gamma_{A,a}$), we take every unique tuple for the sets $\xi_h \in \{1.0, 2.0, 3.0\}$, $\xi_R \in \{D/8, D/4, 3D/4, D/2\}$, and $\theta_c \in \{1.047, 0.785, 0.654, 0.572, 0.471, 0.368, 0.276, 0.186, 0.092\}$ along both the minor and major axes. Any structure function in which any plane in any pillar of a given diameter was found to be not a number was not used to fit any plane weakness or subsequent fluctuation models. This condition occurs rarely for softness structure functions when few monomers are in a given region due to our computational cutoffs. We find that, similar to the particle-level softness field, test set accuracy of plane weakness is insensitive to the exact set of parameters in our calculation so long as the structure of the plane is adequately described.